Carbohydrate Polymers 121 (2015) 477–485

Contents lists available at ScienceDirect

Carbohydrate Polymers

journal homepage: www.elsevier.com/locate/carbpol

Quantum dots loaded nanogels for low cytotoxicity, pH-sensitive fluorescence, cell imaging and drug delivery

Zhenshun Li[a,b], Wei Xu[a], Yuntao Wang[a], Bakht Ramin Shah[a], Chunlan Zhang[a], Yijie Chen[a,c], Yan Li[a,c], Bin Li[a,c,*]

[a] College of Food Science and Technology, Huazhong Agricultural University, Wuhan 430070, China
[b] College of Life Science, Yangtze University, Jingzhou 434025, China
[c] Key Laboratory of Environment Correlative Dietology (Huazhong Agricultural University), Ministry of Education, Wuhan 430070, China

ARTICLE INFO

Article history:
Received 28 July 2014
Received in revised form 1 December 2014
Accepted 3 December 2014
Available online 30 December 2014

Keywords:
Nanogels
Low cytotoxicity
Quantum dots
Cell imaging
Drug delivery

ABSTRACT

Nanogels (NGs) with drug tracking and delivery possess promising usage in clinical treatment. In this study, an available, low toxic and facile approach was developed to synthesize CdTe quantum dots loaded nanogels (QDs-NGs). The QDs-NGs retained the intrinsic pH sensitivity of the QDs with regard to the fluorescence intensity. The QDs-NGs were easily internalized by the cells as fluorescence probes, and acted as carriers for delivering methotrexate (MTX). The cellular uptake indicated that the QDs-NGs can protect QDs from decomposition in cytoplasm and retain the native fluorescence intensity. MTT assay demonstrated that the QDs-NGs greatly decreased the cytotoxicity of the QDs. The MTX loaded QDs-NGs exhibited slow release property in PBS buffer. Moreover, the MTX loaded QDs-NGs distinctly enhanced the availability of drug. The QDs-NGs are potential nanocarriers for the cell imaging and drug delivery.

1. Introduction

The development of multifunctional nanomaterials combining diagnostic and therapeutic purpose has recently attracted great interest (Huang et al., 2014). To detect and track drug-loaded carriers in biological systems, fluorophores are usually conjugated to the carriers. However, quantum dots (QDs), a sort of inorganic fluorescent probes, are gaining much attention in clinical applications. QDs possess advantages such as high quantum yields and robust fluorescence, easy control of surface functionality, and resistance to both chemical and photo-irradiation degradation, which are critical for long time tracking research in vivo. CdTe QDs, which possess high photoluminescence quantum yields (PLQY) (~84%) (Sheng, Han, Hu, & Chi, 2010) and tunable emission peaks from 500 to 650 nm, have been playing an important role in biological applications (Shi, Liu, & Su, 2014). However, a few QDs, especially CdTe and CdSe QDs, may have cytotoxicity (Chen et al., 2012).

Many attempts were made for reducing the cytotoxicities and finding the substitutions for heavy mental-based QDs. Up to now, non-toxic elements such as zinc, sulfur and copper were often used (Kur-Kowalska, Przybyt, Ziolczky, Sowinski, & Miller, 2014; Tan, Huang, Peng, Tang, & Li, 2014). Carbon dots and noble metal nanoclusters were also pursued as possible alternatives in the field of cell imaging (Chong et al., 2014; Su, Wang, Liu, Wu, & Nie, 2013). However, low PLQY and limited signal sensitivity were the main concerns.

Recently, it was reported that the cytotoxicity of CdTe QDs not only comes from the release of Cd^{2+} ions but also the intracellular distribution of QDs in cells (Chen et al., 2012). In addition, the surface stabilizers and particle size also influence cytotoxicity (Kuzyniak et al., 2014; Ryman-Rasmussen, Riviere, & Monteiro-Riviere, 2007; Zhu, Li, Chen, Cooper, & Xu, 2013). However, there are sparse examples for lowering the cytotoxicity of Cd^{2+}-based QDs with reducing the release of Cd^{2+} and free QDs.

Abbreviations: QDs, quantum dots; NGs, nanogels; QDs-NGs, quantum dots loaded nanogels; MTX, methotrexate; PLQY, photoluminescence quantum yields; MTX-QDs-NGs, methotrexate loaded QDs-NGs; Ly, lysozyme; CMC, carboxymethylcellulose; TGA, thioglycolic acid; DMEM, Dulbecco's modified Eagle's medium; IMDM, Iscove's modified Dulbecco's medium; FBS, fetal bovine serum; MTT, [3-(4, 5-dimethylthiazol-2-yl)-2,5-diphenyltetrazolium bromide]; DMSO, dimethylsulfoxide; TEM, transmission electron microscopy; PDI, polydispersity index; XPS, X-ray photoelectron spectroscopy; FTIR, Fourier transform infrared spectroscopy; XRD, X-ray diffraction; EE, encapsulation efficiency; LC, loading capacity; RLS, resonance light-scattering.

* Corresponding author at: College of Food Science and Technology, Huazhong Agricultural University, Wuhan 430070, China. Tel.: +86 27 63730040; fax: +86 27 87282966.
E-mail address: libinfood@mail.hzau.edu.cn (B. Li).

http://dx.doi.org/10.1016/j.carbpol.2014.12.016
0144-8617/

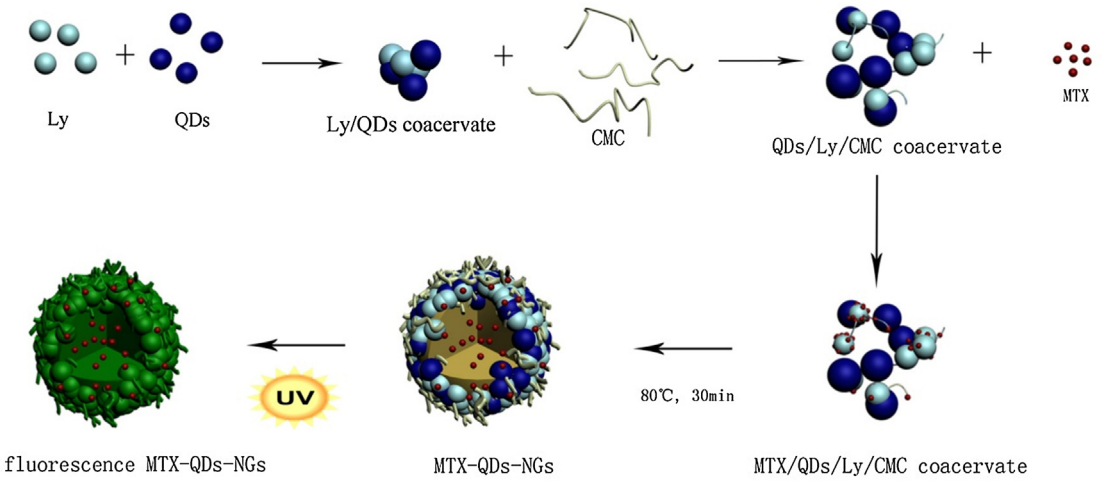

Scheme 1. The preparation process of MTX-QDs-NGs based on Ly and CMC.

In this paper, using CdTe QDs as model Cd^{2+}-based QDs, a simple, cheap and green method was developed to prepare CdTe QDs loaded nanogels (QDs-NGs). Natural polymers were often used as materials of carriers for delivery application because of excellent biocompatibility (Chen, Remondetto, & Subirade, 2006; Hu, Ting, Zeng, & Huang, 2012; Yang, Zhou, & Chen, 2014; Yao et al., 2013). Lysozyme (Ly) and carboxymethylcellulose (CMC) were selected as model protein and polysaccharide to prepare nanogels. Schematic diagram of methotrexate (MTX) loaded QDs-NGs formation is shown in Scheme 1. The electrostatic interaction among Ly, CMC, QDs and MTX was the main driving force to produce MTX loaded QDs-NGs. The QDs-NGs presented much lower cytotoxicity compared with free QDs, and excellent fluorescent cell imaging property. Moreover, the drug bioavailability of MTX was improved after encapsulation by QDs-NGs. The results indicate that it was a new strategy to assemble natural polymers on QDs for cell imaging as well as drug carrier in cancer therapy.

2. Materials and methods

2.1. Materials

Lysozyme (Ly), carboxymethylcellulose (CMC) (degree of esterification 0.7, average molecular weight 90,000), methotrexate (MTX), cadmium chloride, thioglycolic acid (TGA), sodium tellurite, trisodium citrate, and sodium borohydride were purchased from Sinopharm Chemical Reagent Co., Ltd., China. Dulbecco's modified Eagle's medium (DMEM), Iscove's modified Dulbecco's medium (IMDM), fetal bovine serum (FBS), penicillin–streptomycin mixtures, and trypsin–EDTA were purchased from Gibco (Carlsbad, CA, USA). [3-(4, 5-dimethylthiazol-2-yl)-2, 5-diphenyltetrazolium bromide] (MTT) and dimethylsulfoxide (DMSO) were purchased from Sigma–Aldrich. All other chemicals were of analytical grade. Aqueous solutions were prepared using ultrapure water with a resistance of 18.2 MΩ cm.

2.2. Preparation of CdTe QDs

Water-soluble TGA capped CdTe QDs were synthesized using one-step way with slight modification (Sheng et al., 2010). In typical experiments, 1.0×10^{-3} mol cadmium chloride was dissolved in 100 ml ultrapure water at a 250 ml round bottom flask with magnetic stirring. Then 1.2×10^{-3} mol TGA was added into the mixture, and the pH was adjusted to 11.0. Finally, 1.5×10^{-3} mol trisodium citrate, 2.0×10^{-4} mol sodium tellurite, 9.6×10^{-4} mol sodium borohydride were successively added into the solution with continuous stirring. After it turned into pale green, the mixture was refluxed at 100 °C for 1.5 h. All the reactions were executed at ambient atmosphere. The as-prepared QDs was deposited with the same volume of alcohol, dried under nitrogen atmosphere, and redissolved in the same volume of ultrapure water. The fluorescence quantum yield of the QDs was calculated as given in the previous report (Lovric et al., 2005).

2.3. Preparation of CdTe QDs loaded nanogels (QDs-NGs)

Ly and CMC were dissolved in ultrapure water with slight magnetic stirring for 4 h at room temperature (25 °C) with the same concentration of 1.0 mg/ml. Then, 2 ml QDs solution (3.5×10^{-5} M) was added to 10 ml Ly solution with magnetic stirring. The mixture of QDs and Ly was dropped into 3 ml CMC solution with vigorous stirring, and the pH was adjusted from initial value (6.7) to 10.5. At end, the samples were heated at 80 °C for 30 min to form QDs-NGs through heat denaturation of Ly.

2.4. Characterization

The morphology of QDs-NGs was observed by using transmission electron microscopy (TEM) (H-7650, Hitachi, Japan). The particle size, polydispersity index (PDI) and zeta potential were determined by using ZetaSizer Nano series (Nano-ZS, Malvern Instruments Ltd., Malvern, UK) at 633 nm with scattering angle of 173°. The fluorescence spectra were detected by using a fluorescence spectrometer (RF-5301PC) with the excitation wavelength of 370 nm, excitation slit width of 3 nm and emission slit width of 1.5 nm. X-ray photoelectron spectroscopy (XPS) measurements were performed with VG Multilab 2000 X-ray Photoelectron Spectrometer. Fourier transform infrared spectroscopy (FTIR) measurements were carried out on a NEXUS 470 spectrophotometer in the range of 4000–500 cm^{-1} at a resolution of 4 cm^{-1}. X-ray diffraction (XRD) measurements were performed with D/Max-IIIA XRD analyzer with Cu Kα radiation (λ = 0.15418 nm), a voltage of 30 kV, an electricity of 50 mA and a scanning rate of 1°/min.

2.5. Subcellular localization of QDs-NGs

Human hepatoma carcinoma cells (HepG2 cells) were cultured in 1 ml DMEM complete media (FBS 10% and penicillin–streptomycin mixtures 1%) in glass bottom dishes at a density of 1×10^4 per dish at 37 °C and 5% CO_2 under sterile conditions.

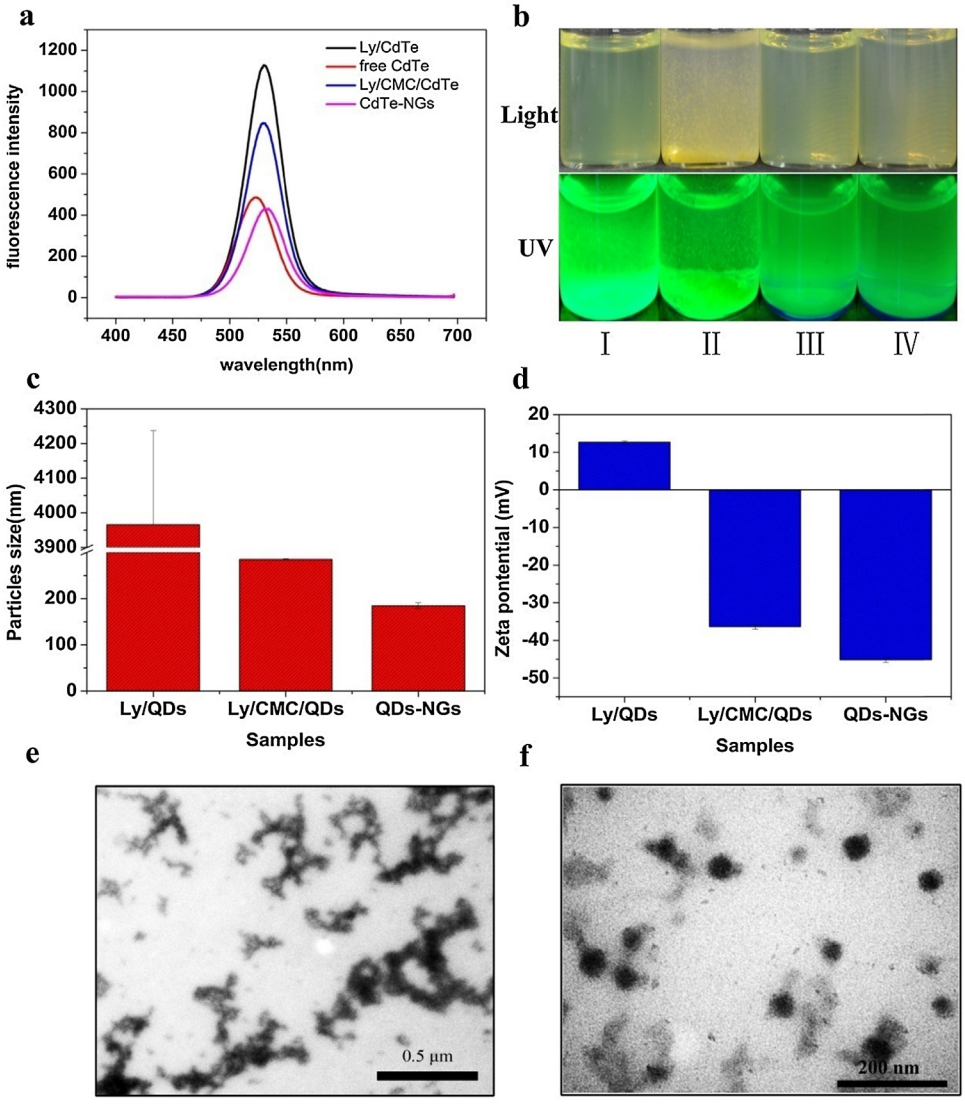

Fig. 1. (a) The fluorescence emission wavelengths of the samples. (b) The optical photographs of the samples under the daylight and UV. Sample name: (I) Ly/QDs coacervates before heating; (II) Ly/QDs coacervates after heating; (III) Ly/CMC/QDs coacervates before heating; (IV) QDs-NGs. (c) Particle sizes of Ly/QDs, Ly/CMC/QDs and QDs-NGs. (d) Zeta potentials of Ly/QDs, Ly/CMC/QDs and QDs-NGs. (e) The TEM image of Ly/CMC/QDs coacervates before heating. (f) The TEM image of QDs-NGs (Ly/CMC/QDs coacervates after heating). The concentrations of QDs, Ly and CMC in all of the samples were consistent, respectively. The pH of all the samples was 9.0.

Multi-drug resistance human breast cancer cells (MCF-7 cells) were cultured in 1 ml IMDM complete media (FBS 10% and penicillin–streptomycin mixtures 1%) at the same culture condition. After culturing for 24 h, HepG2 and MCF-7 cells were replaced with basal culture media containing QDs-NGs (concentration of 480 nM) respectively, and successively cultured for 1–12 h. Ultimately, the samples, washed with PBS for three times, were imaged by confocal laser scanning microscopy equipped with an ultraVIEW Vox confocal attachment (Carl Zeiss, LSM510 META, Germany).

2.6. Drug encapsulation

The QDs were added into Ly solution, and the mixture was dropped into CMC solution through the same process as for the preparation of QDs-NGs. Then the MTX solution (10 mg/ml, dissolved by 0.1 mol/L sodium hydroxide) was added into the mixture of Ly, CMC and QDs to reach the final concentration of 150 μg/ml. After the pH was adjusted from 8.5 to 10.5, the solutions were heated at 80 °C for 30 min. Finally, the MTX-QDs-NGs were centrifuged in ultrafilters with molecular cutting off of 10,000 Da at 4000 r/min for 30 min. MTX in the filtrate as unloaded section was determined by a UV-vis spectrophotometer (UV-1100, MAPADA) at 303 nm. The encapsulation efficiency (*EE*) and loading capacity (*LC*) were calculated as follows:

$$EE = \frac{\text{total weight of MTX} - \text{weight of unloaded MTX}}{\text{total weight of MTX}} \times 100\%$$

$$LC = \frac{\text{total weight of MTX} - \text{weight of unloaded MTX}}{\text{weight of QDs-NGs}} \times 100\%$$

2.7. In vitro drug release

Drug release was evaluated using dialysis method. Briefly, 10 ml of prepared QDs-MTX-NGs and the same concentration of free MTX were respectively placed into dialysis bags (MWCO 8∼14 kDa) and dialyzed with 100 ml of PBS buffer (pH 7.4) in a water bash shaker at 100 r/min for 24 h. At defined time intervals aliquots of 1 ml were collected and freshly prepared PBS of equal volume was added every time. The collected aliquots were determined by UV–vis spectrophotometry at 303 nm as the release amount of MTX drug.

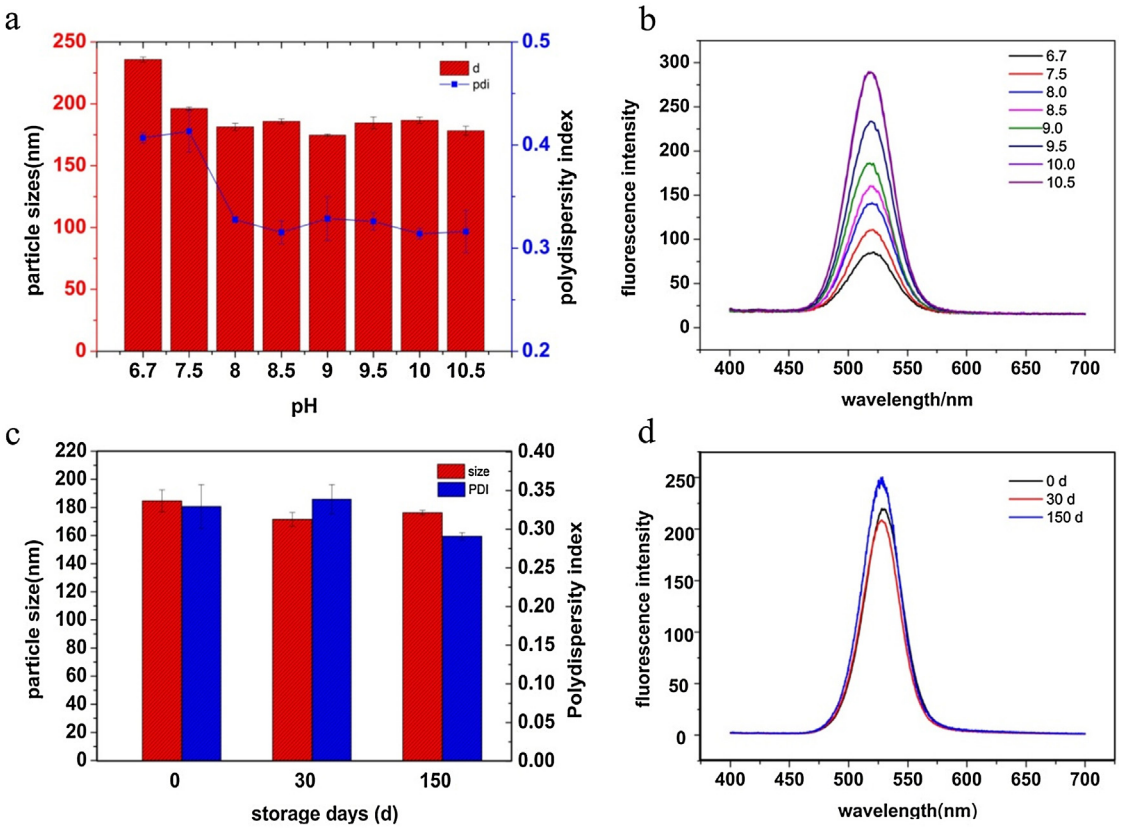

Fig. 2. (a) The particle size and PDI of QDs-NGs at different pH preparation condition; (b) the fluorescence intensity of QDs-NGs at different pH preparation condition; (c) the particle size and PDI of QDs-NGs at different store time; (d) the fluorescence intensity of QDs-NGs at different store time.

2.8. Cytotoxicity assay

HepG2 cells and MCF-7 cells were used for cytotoxicity assay. HepG2 cells were cultured in DMEM complete medium; and MCF-7 cells were cultured in IMDM complete medium. The HepG2 cells and MCF-7 cells in logarithmic phase were seeded in 96-well plate at a density of 1×10^4 cells per well in 100 μl complete media and grown for overnight. The culture media were replaced with 100 μl of basal media containing tested materials, and the cells were further cultivated for 24 h. The media were replaced with 100 μl basal media again and the cells were cultivated for another 24 h to test the chronic cytotoxicity of QDs absorbed by the cells. Therefore, the total incubation time was 48 h. Then, the media were replaced with 200 μl of basal media containing 0.5 mg/ml MTT and continued incubating for 4 h. At last, the media were replaced with 150 μl of DMSO to dissolve the formazan crystals. The absorbance was measured with a microplate reader at 570 nm.

2.9. Statistical analysis

All data were presented as the mean ± standard deviation of three independent experiments. Comparisons were performed using a two-tailed paired Student's *t* test ($^*p < 0.05$, $^{**}p < 0.01$).

3. Result and discussion

3.1. The preparation of QDs loaded NGs

The interactions of TGA capped CdTe QDs (PLQY 73%), Ly and CMC were analyzed by using fluorescence property, particle size, zeta potential and TEM (Fig. 1). The electrostatic interaction produced between QDs and Ly when the pH was below the isoelectric point of Ly. The fluorescence intensity of QDs was greatly enhanced after blending with Ly because the electrostatic interaction between the CdTe quantum dots and lysozyme increased the size and light scattering section of the complex (Fig. 1a) (Li, He, Wu, Li, & Zhang, 2007). The similar result was observed in Fig. 1b I. However, the visible aggregation formed after thermal treatment (Fig. 1b II), because of the unstable Ly/QDs coacervates with large particle size (3966 ± 271.17 nm) and small surface charges (12.7 ± 0.30 mV). CMC was introduced to the Ly/QDs coacervates for increasing the stability of the system through electrostatic interaction. Then stable Ly/CMC/QDs coacervates were obtained with strong negative charges (−36.37 ± 0.65 mV) and small particle size (285.03 ± 0.93 nm). Meanwhile, the fluorescence was quenched when CMC was introduced in the Ly/QDs coacervates, probably because large aggregations were formed among CMC, Ly and QDs. Moreover, the fluorescence intensity was further decreased after thermal treatment. Additionally, the emission peak shifted toward long wavelength, probably due to the aggregation of embedded QDs (Li, Zhang, et al., 2007). And the particle size was decreased, perhaps because of the shrinkage of the coacervates.

Irregularly shaped Ly/CMC/QDs coacervates were initially observed from TEM image before heating (Fig. 1e). However, the spherical QDs-NGs formed after heating (Fig. 1f). It was reported that the thermal treatment of the Ly and CMC coacervates could enhance the gel property (Zhu, Ye, et al., 2013). Because Gel is an excellent material for loading and slow releasing bioactive molecules for its semipermeability (Byun & Lee, 2014), the QDs-NGs may have potential usage as nanocarriers.

For evaluating the encapsulation efficiency of QDs, the QDs-NGs solution was centrifuged in an ultrafilter with molecular cutting

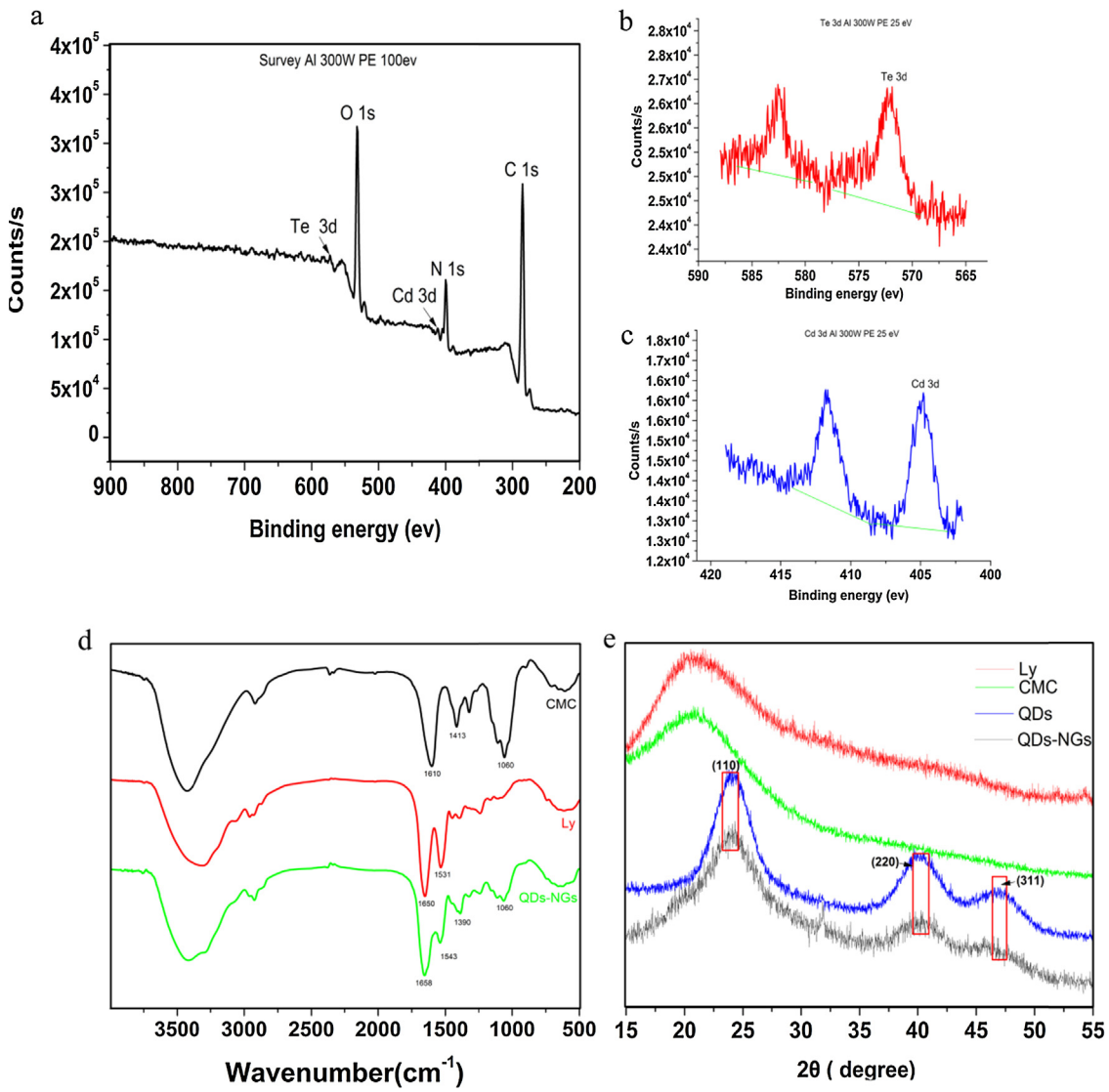

Fig. 3. The characterization of the QDs-NGs: (a) XPS patterns of QDs-NGs; (b) XPS spectrum of Te 3d narrow scans; (c) XPS spectrum of Cd 3d narrow scans; (d) FTIR spectra of CMC, Ly and QDs-NGs; (e) XRD spectra of CMC, Ly, QDs and QDs-NGs.

off of 50,000 Da (the molecular weight of QDs was 16,000 Da) at 4000 r/min for 30 min. There was not any fluorescent signal detected from the filtrate, which indicated that almost all the QDs were encapsulated in the NGs (result was not shown). The loading capacity of the NGs was (10.1 ± 0.8)%.

3.2. The stability of QDs-NGs

The pH is one of the most critical factors in preparing NGs because it effects the charge distribution of materials which possess opposite charges (Jones, Decker, & McClements, 2009, 2010). The particle size and PDI at different pH preparation were presented in Fig. 2a. When the pH value was 6.7, which was far away from the isoelectric point (10.7) of Ly, there was strong electrostatic interaction between Ly and CMC molecules, resulting in larger particle size (Zhang, Hsieh, & Vardhanabhuti, 2014). When the pH values increased from 8.0 to 10.5, the particle size and PDI reached minimum first and remained stable, perhaps because the reduced electrostatic interaction led to less aggregation. At the same time, other forces such as hydrogen bonds and hydrophobic interactions between Ly and CMC might produce during assembling, which resulted in the stable particle size when the pH was further increased. It was interesting to note that the fluorescence intensities were gradually enhanced with increasing the pH (Fig. 2b). The results manifested that the QDs-NGs still retained the native fluorescent pH sensitivity of TGA capped CdTe QDs (Sorouraddin, Imani-Nabiyyi, Najibi-Gehraz, & Rashidi, 2014; Yang et al., 2011), because the physical bond between QDs and polymers does not destroy the structure of the QDs. The pH values before and after heating were shown in Table S1.

The good storage stability of biomaterials is crucial for practical applications. For testing the stability of the QDs-NGs, they were stored at 4 °C for 150 days (Fig. 2c,d). The particle size, PDI and fluorescence intensity were not affected during storage. The wonderful storage stability was probably due to the strong negative charges (−45.16 ± 0.67 mV; Fig. 1d) and antibacterial materials of Ly and QDs (Kumar, Srivastava, & Dutta, 2013).

3.3. The characterization of QDs-NGs

XPS was employed to analyze the information on the electronic state of the surface region of samples. A wide survey XPS spectrum (Fig. 3a) of the QDs-NGs showed that NGs mainly consist of carbon (70.41%), oxygen (18.11%), nitrogen (10.7%), and a handful of S

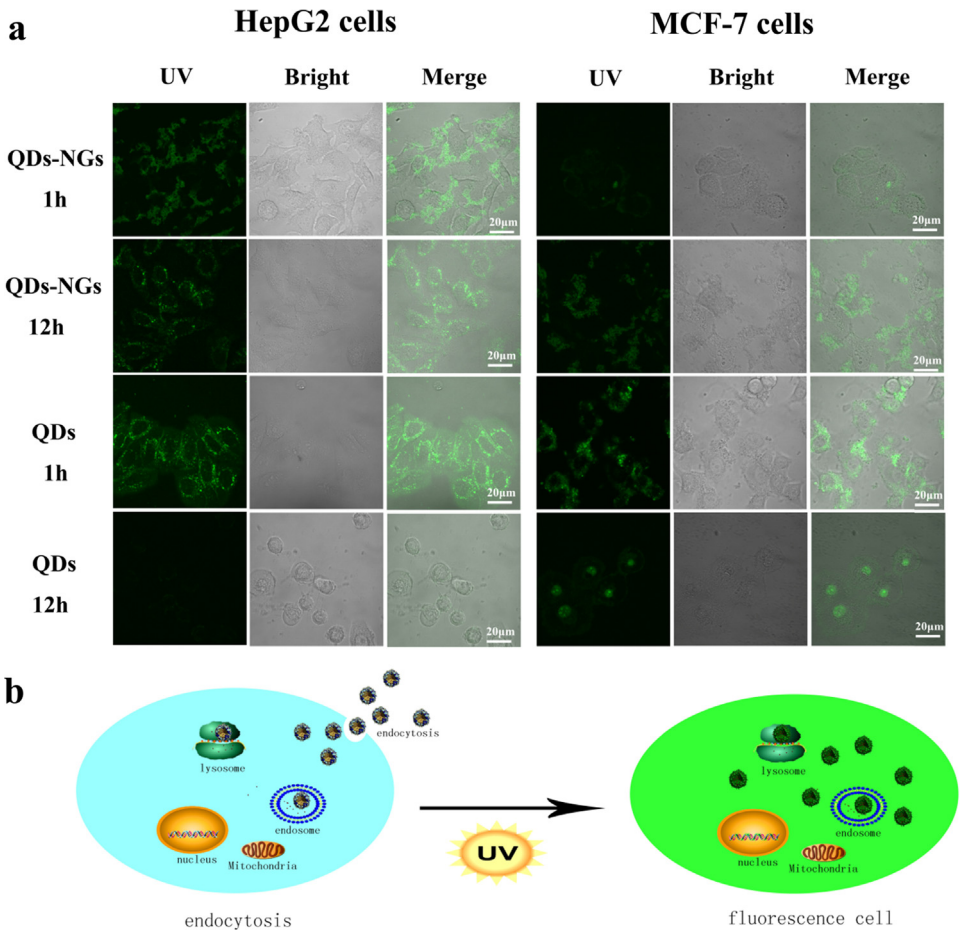

Fig. 4. (a) Intracellular delivery of free QDs and QDs-NGs in HepG2 and MCF-7 cells with incubation for 1 h and 12 h. (b) Schematic diagram of endocytosis to QDs-NGs and fluorescence cells.

(0.84%), Te (0.19%), and Cd (0.29%). The high-resolution XPS spectra of the QDs-NGs showed peaks at binding energy of 404.83 eV for Cd 3d (Fig. 3b), and binding energy near 572.13 eV for Te 3d (Fig. 3c). The contents of carbon and oxygen in curves of Ly and CMC were 67.88%, 17.6% and 60.23%, 39.36% respectively (Xu et al., 2014). The nitrogen (13.74%) only existed in Ly, as concluded from the results of our laboratory (Zhu, Ye, et al., 2013). Overall, these results suggest that the shell of QDs-NGs constitute the mixture of CMC, Ly and QDs, as highlighted in Scheme 1.

In the FTIR spectrum of CMC, the absorption bands between 1000 and 1200 cm^{-1} were characteristic of —C—O— stretching (Fig. 3d). The two peaks at 1413 and 1610 cm^{-1} corresponded to the symmetrical and asymmetrical stretching vibrations of the carboxylate groups (Chang, Yu, Ma, & Anderson, 2011). The peak at 1060 cm^{-1} was attributed to C—C bond. While in the Ly FTIR spectrum, the peak at 1650 cm^{-1} was due to the stretching of the conjugated peptide bond formed by amine (NH) and acetone groups (Barreca et al., 2014). The peak at 1531 cm^{-1} in the Ly FTIR spectrum was secondary NH bending (Subia & Kundu, 2013). However, in the FTIR spectrum of QDs-NGs, there were obviously shifted peaks among groups. The peaks of symmetrical stretching vibrations of the carboxyl groups in CMC were shifted from 1413 cm^{-1} to 1390 cm^{-1}. Meanwhile, the peak of secondary NH bending of Ly was shifted from 1531 cm^{-1} to 1543 cm^{-1}, because of strong electrostatic interaction between carboxyl groups of CMC, TGA capped CdTe QDs and amino groups of Ly. The peak at 1658 cm^{-1} of QDs-NGs was the overlay of carboxylate groups at 1610 cm^{-1} of CMC and the peptide peak at 1650 cm^{-1} of Ly spectrum. The intensity of 1060 cm^{-1} peak in QDs-NGs was greatly weakened compared with CMC, due to the decreasing mass ratio of CMC in QDs-NGs.

The XRD profiles were used to analyze the crystallization of materials. The broad peaks observed in the XRD patterns of Ly and CMC at 2θ about 20° are attributed to the highly disordered carbonaceous materials (Devi & Kannan, 2007) in CMC and Ly (Fig. 3e). On the other hand, the same peaks appeared on the patterns of QDs and QDs-NGs at 24.0°, 40.3° and 46.9°, which were consisted with the previous results about (1 1 1), (2 2 0) and (3 1 1) planes of TGA capped CdTe QDs (Yang et al., 2011). The results demonstrated that the native QDs crystallization was retained in the QDs-NGs.

3.4. Fluorescence cellular imaging

Cellular uptake of QDs-NGs were demonstrated on HepG2 and MCF-7 cell lines using confocal laser scanning microscopy (Fig. 4a). The pictures showed that free QDs and QDs-NGs were all internalized by both of the cell lines. The fluorescence intensities of the cells in free QDs samples were greater than those in QDs-NGs samples at incubation for 1 h. Noteworthily, the fluorescence intensity of MCF-7 cells was lower than that of HepG2 cells because MCF-7 cells were coated with hyaluronic acid which could block the access of materials to the cell surface (Yang et al., 2013). It was reported that the particle size is one of the most important factors which influence the internalization and cytotoxicity (Chen & von Mikecz, 2005; Zhu, Li, et al., 2013). Therefore, the

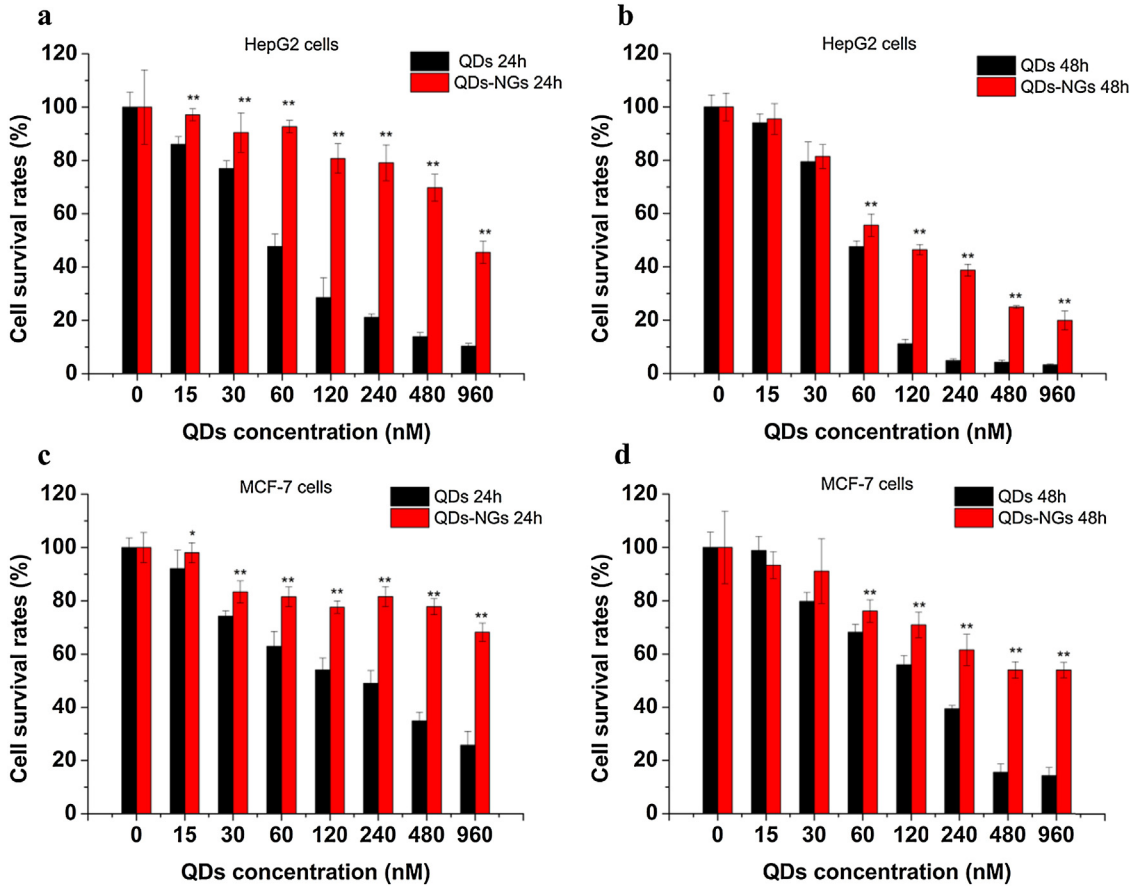

Fig. 5. Viability of cells after 24 h of exposure to QDs and QDs-NGs: (a) HepG2 cells; (c) MCF-7 cells. Viability of cells at incubation for 48 h: (b) HepG2 cells; (d) MCF-7 cells. The QDs concentrations in both free QDs and QDs-NGs were from 15 to 960 nM and equal in each group.

obtained QDs with much smaller particle size (2.3 nm) was easily absorbed by the cells than the QDs-NGs. However, after incubation for 12 h, the fluorescence of both cell lines with free QDs incubation was sharply quenched. Besides, it was obvious to see that the QDs were predominantly distributed in the nuclear of MCF-7 cells wih free QDs incubation because the small particle size of QDs easily penetrated into cell nuclear and caused cytotoxicity. In comparison, the green fluorescence was clear to see at cytoplasm in both of the cell lines at the QDs-NGs groups because the QDs coated by polymers can protect QDs from degradation in cytoplasm. The QDs-NGs were internalized by the cells through the process of endocytosis (Subia & Kundu, 2013). Further research is necessary to understand the mechanism of endocytosis. It was reported that P-glycoprotein at the cancerous cell membrane can increase the efflux of various hydrophobic anticancer drugs (Mussi et al., 2014). The QDs-NGs can be used as drug carriers to bypass the P-glycoprotein bomb efflux of MCF-7 cells and reach the cytoplasm. The schematic diagram of cellular imaging was shown in Fig. 4b.

3.5. Cytotoxicity of QDs-NGs

The particle size of nanoparticles affected their cell-uptake and cytotoxicity (Zhu, Li, et al., 2013). The larger particle size of QDs-NGs causes the slower endocytosis than free QDs and relieves the toxic effect. Moreover, the polymers shell can inhibit the release of free QDs and toxic Cd^{2+} and thus reduce QDs' toxicity (Derfus, Chan, & Bhatia, 2004). In fact, the cytotoxicity of QDs-NGs was greatly decreased compared with free QDs in Fig. 5. Besides, it was clear to see that the QDs-NGs were more lethal to HepG2 cells than MCF-7 cells, probably because of the lesser absorption of QDs-NGs in MCF-7 cells, resulted from the fluorescence cellular imaging. The viabilities exhibited the concentration-dependent manner in free QDs groups at both of the cell lines. Nevertheless, the viabilities of both cell lines in QDs-NGs samples were less affected than which in free QDs. It is agreed with the results of fluorescence cellular imaging. Chronic toxicity was tested after further 24 h incubation. The results indicated that both of the free QDs and QDs-NGs all exhibited chronic toxicity. However, the viabilities of both of the cell lines incubated with QDs-NGs were all significantly higher than which incubated with free QDs. The results illustrated that the QDs-NGs can effectively decrease the cytotoxicity. Even though these results were preliminary and more extensive toxicity studies in animal models are needed to further ascertain their safety, yet they are satisfactorily encouraging to support the application of the QDs-NGs in drug delivery.

3.6. Drug loading and in vitro drug release

Taking into account all these promising results, the potential application of QDs-NGs as a drug delivery carrier was explored. MTX was used as a model drug to demonstrate the drug delivery function of the QDs-NGs. The electrostatic interaction and hydrophobic interaction between MTX and Ly might contribute the main assemble force. The entrapment efficiency (*EE*) and loading capacity (*LC*) at different pH values were shown in Table S2. *EE* and *LC* reached the maximum (55.25% and 10.90% respectively) at pH 9.5.

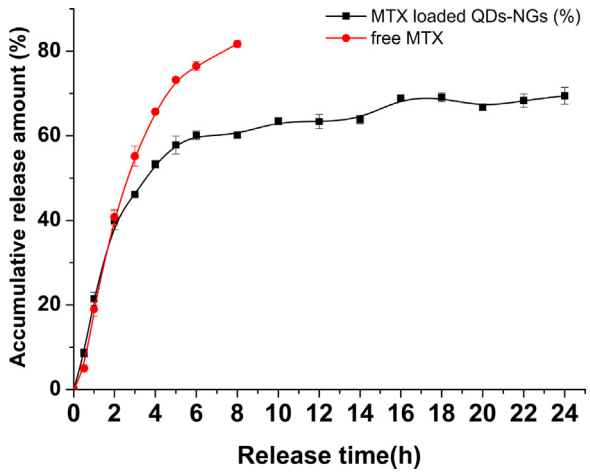

Fig. 6. Accumulative release profiles of MTX from MTX loaded QDs-NGs.

A drug remained at the site of action in body for a long period of time could be advantageous to sustain release. The accumulative release research of MTX from the MTX-QDs-NGs was conducted in PBS buffer (pH 7.4) at 37 °C in Fig. 6. As the control, the release curve of free MTX was much steeper than the MTX-QDs-NGs sample, which indicated the burst release of free MTX. Such trend is also noticed in MTX-QDs-NGs but after 2 h there was more steady release that saturates at around 24 h. The presence of unincorporated drug molecules located at the QDs-NGs surface might be responsible for the observed burst effect. In the following period, the driving forces of releasing MTX from the QDs-NGs may be the swelling of the QDs-NGs (Hu, Ting, Zeng, & Huang, 2013), the drug effusion from the interior of the QDs-NGs and the erosion of the NGs (Zhu, Ye, et al., 2013). Overall, these results suggest that QDs-NGs could be advantageous for encapsulation and sustained release of anti-cancer drugs such as MTX as well as other disease preventing compounds.

3.7. In vitro cytotoxicity

To determine the anticancer activity of free MTX and MTX-QDs-NGs, MTT assay was performed on HepG2 cells and MCF-7 cells. The cells cultured in media were taken as control with a cell viability of 100%. MTX exhibited great growth inhibition to HepG2 cells with increasing the drug concentrations (Fig. 7a). However, free MTX had little effect on the cell viability of MCF-7 cells from the results in Fig. 7b, because the multidrug resistance MCF-7 cells were well known to resist widely anticancer drugs such as MTX, paclitaxel, 10-hydroxycamptothecin, etc. (Zhou et al., 2013). It is noteworthy that a remarkable decrease in viability of both cell lines treated with MTX-QDs-NGs was detected in comparison with free MTX at the same drug concentrations. It was probably because the nanogels may enter into the cancerous cells through an endocytosis mechanism (Fig. 7c), which was in accordance with the previous report (Subia & Kundu, 2013). The results also agreed with other reports that nanogels as carriers were able to reduce multidrug resistance by a mechanism of internalization of the drug, reducing drug efflux from cells by P-glycoprotein mediation (Zhu et al., 2014). It was reported that nanocarriers which increased the availability of cancer drugs can retain localizing in the endosomes/lysosomes of the cells and gradually release the drug within the cells (Fig. 7c) (Zhang, Neoh, et al., 2014). Thus, MTX loaded QDs-NGs are hopeful nanocarriers for reducing the dosing frequency and increasing patient compliance during chemotherapy.

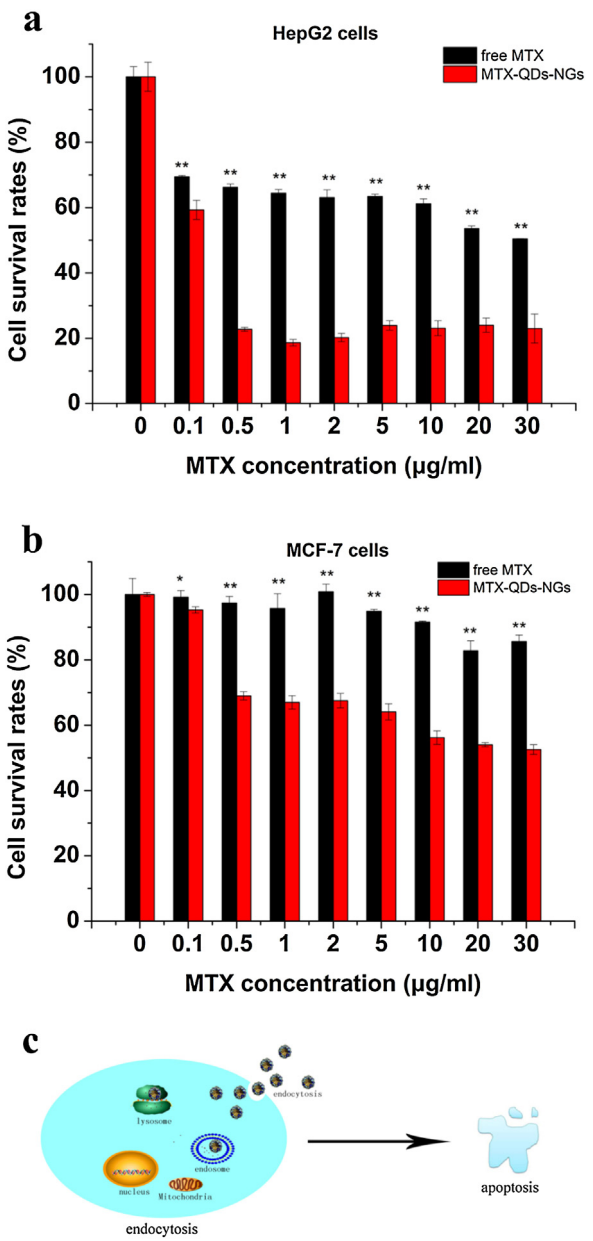

Fig. 7. Cytotoxic effects of free MTX and MTX-QDs-NGs. (a) HepG2 cells; (b) MCF-7 cells. c) Schematic diagram of endocytosis to QDs-NGs and apoptosis.

4. Conclusions

QDs loaded NGs were fabricated in a simple and green method. The cytotoxicity of QDs-NGs was much reduced compared to free QDs. In addition, the MTX entrapped QDs-NGs can enhance the anticancer activity of the drug. The preparation of QDs-NGs provides a new way to reduce the cell toxicity of Cd^{2+}-based QDs. The results suggested that the obtained QDs-NGs can be used as drug carriers and fluorescence probes in clinical therapy.

Acknowledgements

This work was financially supported by the National Natural Science Foundation of China (Grant No. 31371841). In addition, we would like to thank classmates and teachers of Key Laboratory of Environment Correlative Dietology of Huazhong Agricultural University for offering many conveniences of the experiments.

Appendix A. Supplementary data

Supplementary data associated with this article can be found, in the online version, at http://dx.doi.org/10.1016/j.carbpol.2014.12.016.

References

Barreca, D., Laganà, G., Magazù, S., Migliardo, F., Gattuso, G., & Bellocco, E. (2014). FTIR, ESI-MS, VT-NMR and SANS study of trehalose thermal stabilization of lysozyme. *International Journal of Biological Macromolecules*, *63*, 225–232.

Byun, E., & Lee, H. (2014). Enhanced loading efficiency and sustained release of doxorubicin from hyaluronic acid/graphene oxide composite hydrogels by a mussel-inspired catecholamine. *Journal of Nanoscience and Nanotechnology*, *14*(10), 7395–7401.

Chang, P. R., Yu, J., Ma, X., & Anderson, D. P. (2011). Polysaccharides as stabilizers for the synthesis of magnetic nanoparticles. *Carbohydrate Polymers*, *83*(2), 640–644.

Chen, L. Y., Remondetto, G. E., & Subirade, M. (2006). Food protein-based materials as nutraceutical delivery systems. *Trends in Food Science & Technology*, *17*(5), 272–283.

Chen, M., & von Mikecz, A. (2005). Formation of nucleoplasmic protein aggregates impairs nuclear function in response to SiO_2 nanoparticles. *Experimental Cell Research*, *305*(1), 51–62.

Chen, N., He, Y., Su, Y., Li, X., Huang, Q., Wang, H., et al. (2012). The cytotoxicity of cadmium-based quantum dots. *Biomaterials*, *33*(5), 1238–1244.

Chong, Y., Ma, Y., Shen, H., Tu, X., Zhou, X., Xu, J., et al. (2014). The *in vitro* and *in vivo* toxicity of graphene quantum dots. *Biomaterials*, *35*(19), 5041–5048.

Derfus, A. M., Chan, W. C. W., & Bhatia, S. N. (2004). Probing the cytotoxicity of semiconductor quantum dots. *Nano Letters*, *4*(1), 11–18.

Devi, T. G., & Kannan, M. (2007). X-ray diffraction (XRD) studies on the chemical states of some metal species in cellulosic chars and the Ellingham diagrams. *Energy & Fuels*, *21*(2), 596–601.

Hu, B., Ting, Y., Zeng, X., & Huang, Q. (2012). Cellular uptake and cytotoxicity of chitosan–caseinophosphopeptides nanocomplexes loaded with epigallocatechin gallate. *Carbohydrate Polymers*, *89*(2), 362–370.

Hu, B., Ting, Y., Zeng, X., & Huang, Q. (2013). Bioactive peptides/chitosan nanoparticles enhance cellular antioxidant activity of (−)-epigallocatechin-3-gallate. *Journal of Agricultural and Food Chemistry*, *61*(4), 875–881.

Huang, H., Li, Y., Sa, Z., Sun, Y., Wang, Y., & Wang, J. (2014). A smart drug delivery system from charge-conversion polymer–drug conjugate for enhancing tumor therapy and tunable drug release. *Macromolecular Bioscience*, *14*(4), 485–490.

Jones, O. G., Decker, E. A., & McClements, D. J. (2009). Formation of biopolymer particles by thermal treatment of beta-lactoglobulin–pectin complexes. *Food Hydrocolloids*, *23*(5), 1312–1321.

Jones, O. G., Decker, E. A., & McClements, D. J. (2010). Comparison of protein–polysaccharide nanoparticle fabrication methods: Impact of biopolymer complexation before or after particle formation. *Journal of Colloid and Interface Science*, *344*(1), 21–29.

Kumar, H., Srivastava, R., & Dutta, P. (2013). Highly luminescent chitosan-L-cysteine functionalized CdTe quantum dots film: Synthesis and characterization. *Carbohydrate Polymers*, *97*(2), 327–334.

Kur-Kowalska, K., Przybyt, M., Ziolczky, P., Sowinski, P., & Miller, E. (2014). Fluorescence properties of 3-amino phenylboronic acid and its interaction with glucose and ZnS:Cu quantum dots. *Spectrochimica Acta Part A – Molecular and Biomolecular Spectroscopy*, *129*, 320–325.

Kuzyniak, W., Adegoke, O., Sekhosana, K., D'Souza, S., Tshangana, S. C., Hoffmann, B., et al. (2014). Synthesis and characterization of quantum dots designed for biomedical use. *International Journal of Pharmaceutics*, *466*(1), 382–389.

Li, J., He, X.-W., Wu, Y.-L., Li, W.-Y., & Zhang, Y.-K. (2007). Determination of lysozyme at the nanogram level by a resonance light-scattering technique with functionalized CdTe nanoparticles. *Analytical Sciences*, *23*(3), 331–335.

Li, M., Zhang, J., Zhang, H., Liu, Y., Wang, C., Xu, X., et al. (2007). Electrospinning: A facile method to disperse fluorescent quantum dots in nanofibers without Förster resonance energy transfer. *Advanced Functional Materials*, *17*(17), 3650–3656.

Lovric, J., Bazzi, H. S., Cuie, Y., Fortin, G. R. A., Winnik, F. M., & Maysinger, D. (2005). Differences in subcellular distribution and toxicity of green and red emitting CdTe quantum dots. *Journal of Molecular Medicine – JMM*, *83*(5), 377–385.

Mussi, S. V., Sawant, R., Perche, F., Oliveira, M. C., Azevedo, R. B., Ferreira, L. A., et al. (2014). Novel nanostructured lipid carrier co-loaded with doxorubicin and docosahexaenoic acid demonstrates enhanced in vitro activity and overcomes drug resistance in MCF-7/Adr cells. *Pharmaceutical Research*, *31*(8), 1882–1892.

Ryman-Rasmussen, J. P., Riviere, J. E., & Monteiro-Riviere, N. A. (2007). Surface coatings determine cytotoxicity and irritation potential of quantum dot nanoparticles in epidermal keratinocytes. *Journal of Investigative Dermatology*, *127*(1), 143–153.

Sheng, Z., Han, H., Hu, X., & Chi, C. (2010). One-step growth of high luminescence CdTe quantum dots with low cytotoxicity in ambient atmospheric conditions. *Dalton Transactions*, *39*(30), 7017–7020.

Shi, F. P., Liu, S. Y., & Su, X. G. (2014). Dopamine functionalized-CdTe quantum dots as fluorescence probes for L-histidine detection in biological fluids. *Talanta*, *125*, 221–226.

Sorouraddin, M.-H., Imani-Nabiyyi, A., Najibi-Gehraz, S. A., & Rashidi, M.-R. (2014). A new fluorimetric method for determination of valproic acid using TGA-capped CdTe quantum dots as proton sensor. *Journal of Luminescence*, *145*, 253–258.

Su, S., Wang, H., Liu, X., Wu, Y., & Nie, G. (2013). iRGD-coupled responsive fluorescent nanogel for targeted drug delivery. *Biomaterials*, *34*(13), 3523–3533.

Subia, B., & Kundu, S. (2013). Drug loading and release on tumor cells using silk fibroin–albumin nanoparticles as carriers. *Nanotechnology*, *24*(3), 035103–035114.

Tan, L., Huang, C., Peng, R., Tang, Y., & Li, W. (2014). Development of hybrid organic–inorganic surface imprinted Mn-doped ZnS QDs and their application as a sensing material for target proteins. *Biosensors and Bioelectronics*, *61*, 506–511.

Xu, W., Jin, W., Zhang, C., Li, Z., Lin, L., Huang, Q., et al. (2014). Curcumin loaded and protective system based on complex of κ-carrageenan and lysozyme. *Food Research International*, *59*, 61–66.

Yang, C., Liu, Y., He, Y., Du, Y., Wang, W., Shi, X., et al. (2013). The use of HA oligosaccharide-loaded nanoparticles to breach the endogenous hyaluronan glycocalyx for breast cancer therapy. *Biomaterials*, *34*(28), 6829–6838.

Yang, J., Zhou, Y., & Chen, L. (2014). Elaboration and characterization of barley protein nanoparticles as an oral delivery system for lipophilic bioactive compounds. *Food & Function*, *5*(1), 92–101.

Yang, S.-S., Ren, C.-L., Zhang, Z.-Y., Hao, J.-J., Hu, Q., & Chen, X.-G. (2011). Aqueous synthesis of CdTe/CdSe core/shell quantum dots as pH-sensitive fluorescence probe for the determination of ascorbic acid. *Journal of fluorescence*, *21*(3), 1123–1129.

Yao, X., Xu, Q., Tian, D., Wang, N., Fang, Y., Deng, Z., et al. (2013). Physical and chemical stability of gum arabic-stabilized conjugated linoleic acid oil-in-water emulsions. *Journal of Agricultural and Food Chemistry*, *61*(19), 4639–4645.

Zhang, Q., Neoh, K.-G., Xu, L.-Q., Lu, S., Kang, E.-T., Mahendran, R., et al. (2014). Functionalized mesoporous silica nanoparticles with mucoadhesive and sustained drug release properties for potential bladder cancer therapy. *Langmuir*, *30*(21), 6151–6161.

Zhang, S., Hsieh, F.-H., & Vardhanabhuti, B. (2014). Acid-induced gelation properties of heated whey protein–pectin soluble complex (Part I): Effect of initial pH. *Food Hydrocolloids*, *36*, 76–84.

Zhou, M., Zhang, X., Yang, Y., Liu, Z., Tian, B., Jie, J., et al. (2013). Carrier-free functionalized multidrug nanorods for synergistic cancer therapy. *Biomaterials*, *34*(35), 8960–8967.

Zhu, H., Chen, H., Zeng, X., Wang, Z., Zhang, X., Wu, Y., et al. (2014). Co-delivery of chemotherapeutic drugs with vitamin E TPGS by porous PLGA nanoparticles for enhanced chemotherapy against multi-drug resistance. *Biomaterials*, *35*(7), 2391–2400.

Zhu, K., Ye, T., Liu, J., Peng, Z., Xu, S., Lei, J., et al. (2013). Nanogels fabricated by lysozyme and sodium carboxymethyl cellulose for 5-fluorouracil controlled release. *International Journal of Pharmaceutics*, *441*(1–2), 721–727.

Zhu, Y., Li, Z., Chen, M., Cooper, H. M., & Xu, Z. P. (2013). Tuning core-shell SiO_2@CdTe@SiO_2 fluorescent nanoparticles for cell labeling. *Journal of Materials Chemistry B*, *1*(17), 2315–2323.